American Mineralogist, Volume 80, pages 268–279, 1995

The dehydration kinetics and microtexture of analcime from two parageneses

Christina M. B. Line
Department of Earth Sciences, University of Cambridge, Downing Street, Cambridge CB2 3EQ, U.K.
and Institut Laue-Langevin, Avenue des Martyrs, B.P. 156-38042 Grenoble Cedex 9, France
Andrew Putnis, Christine Putnis
Department of Earth Sciences, University of Cambridge, Downing Street, Cambridge CB2 3EQ, U.K.
Ciriaco Giampaolo
Dipartimento di Scienze Geologiche, III Universitá degli Studi di Roma, Via Ostiense 169, 00154 Rome, Italy

Abstract

The dehydration behavior of an analcime formed by ion exchange from leucite (X-type analcime, or secondary analcime) is contrasted with the behavior of an analcime formed by hydrothermal recrystallization from structurally dissimilar materials (hydrothermal analcime, or H-type analcime). The kinetics of dehydration of X-type analcime is consistent with a high specific surface area, showing surface equilibration with H_2O vapor and fast initial H_2O loss. The kinetic data approximately fit the Austin-Rickett equation, yielding an empirical activation energy for the dehydration of X-type analcime of 33 kJ/mol, compared with 92 kJ/mol for H-type analcime. Washed and ultrasonically cleaned samples of the same grain size have very different BET (N adsorption) surface areas, being 20 m^2/g for X-type analcime and 2 m^2/g for H-type analcime, consistent with the high porosity of the surface of X-type analcime, as observed by SEM. Further analysis of the N adsorption data shows the pore size distribution for the X-type analcime to have a maximum at 100 Å. The rate of Na drift under electron microprobe is more than 15 times higher for X-type analcime than for H-type analcime and could be a convenient means of distinguishing the two parageneses.

Introduction

Analcime ($NaAlSi_2O_6 \cdot H_2O$) has been classified both as a zeolite and as a framework mineral. As a zeolite, it is the end-member with the smallest H_2O cage. It has the same framework structure as the framework mineral leucite ($KAlSi_2O_6$), but with one H_2O molecule for each of the 16 large K sites (called cages) and with Na atoms taking up 16 of the 24 smaller sites between cages.

In almost all known cases, analcime forms in hydrothermal conditions. In many of these occurrences, analcime is found as single crystals, a millimeter to a centimeter in size, with well-defined {211} and {100} faces, lining vesicles in the rock. This analcime is inferred to have been formed by dissolution of a structurally dissimilar source material (for example, nepheline, plagioclase, quartz, albite, or volcanic glass) and recrystallization of analcime from the hydrothermal solution. Karlsson and Clayton (1990b) and Giampaolo and Lombardi (1994) referred to it as H-type analcime. In this paper, we will also refer to this paragenesis as H-type analcime.

In the laboratory, analcime is easily synthesized under hydrothermal conditions. The summary by Gottardi and Galli (1985) showed that, within the field of stability of analcime, many heterogenous mixtures of aluminosilicates yield analcime as a single product. Ueda and Koizumi (1979) showed that analcime can form from a clear aqueous solution of an aluminosilicate gel and that it was the composition of the solution rather than the composition of the nucleus that controlled the composition of the analcime. An active ionic species was therefore hypothesized to act as the subunit of the analcime structure.

One special case of an analcime that forms under hydrothermal conditions is when the source material is the mineral leucite ($KAlSi_2O_6$). The framework structure of leucite is identical to that of analcime, the only difference being the cations and the H_2O content. Hence the leucite-analcime reaction involves an ion-exchange process: $KAlSi_2O_6 + NaCl_{aq} + H_2O = NaAlSi_2O_6 \cdot H_2O + KCl_{aq}$. Karlsson and Clayton (1990b) and Giampaolo and Lombardi (1994) call this X-type analcime, in reference to the ion-exchange character and to distinguish it from I-type or igneous analcime. Karlsson and Clayton (1991) also referred to it as secondary analcime to distinguish it from primary igneous analcime. In this paper, we will refer to it as X-type analcime. In nature, this X-type analcime is formed as an in-situ replacement product and can be identified by its texture when found as large powdery aggregates retaining the {211} morphology of single crystals of leucite, with remnants of the original leucite often re-

0003–004X/95/0304–0268$02.00

maining as a core. The leucite-analcime reaction requires hydrothermal conditions, since if the salt solution is too concentrated the reaction does not go to completion (Gupta and Fyfe, 1975). The reaction is very fast, requiring about 3 d at 300 °C and 1 kbar when using 100-μm grains of leucite as the starting material, and the analcime product is of the same apparent grain size. For similar conditions (36–60 h, at 180–270 °C) growth of hydrothermal analcime from solution (H-type analcime) produces grains of 15–20 μm (Barrer and White, 1951, 1952). Thus, from the very large difference in grain size, it would seem unlikely that the X-type analcime has grown by renucleation from solution, as has the H-type analcime.

A possible mechanism for the leucite-analcime reaction is solid-state ion exchange. However, there is a 10% volume increase from leucite to analcime. With leucite grain sizes of 100 μm it is hard to understand how the analcime could form by simple solid-state ion exchange from leucite, while keeping the framework structure intact. The powdery texture of the analcime may result from a breakup of the leucite into small crystals in order to accommodate expansion, but the process would involve large structural strains throughout the crystal. Thus some understanding of the mechanism of the reaction would seem to be of interest.

An important motive in this investigation was to discover ways of distinguishing between H-type and X-type analcime and thereby to contribute to the current debate over the origin of igneous analcime, which Karlsson and Clayton (1990b) called I-type analcime. A summary of this debate appeared in Karlsson and Clayton (1991). It is not certain whether the analcime found in igneous rocks has crystallized directly from the melt, so that analcime can be a primary igneous mineral, or whether it was leucite that was crystallized and subsequently altered at subsolidus temperatures to analcime, so that the analcime found in igneous rocks is in fact secondary after leucite and therefore X type. The difficulty has been that the analcime crystals have the same morphology as leucite and are extremely small, so that texturally they cannot be identified as being X type, and the extremely rapid nature of the leucite-analcime transformation has meant that the lack of leucite in the host rock cannot be taken as evidence for a primary origin of the analcime. The most recent study, which found a difference between the framework O isotope ratios of analcime and that of the host rock (Karlsson and Clayton, 1991), showed that the framework had interacted with fluids but could not determine whether that happened before or after the formation of the analcime, since analcime framework O exchanges readily with the channel H_2O molecule (Karlsson and Clayton, 1990a). The debate has therefore focused on textural and mineralogical analyses of various igneous rocks in which analcime is found (Karlsson and Clayton, 1993; Pearce, 1993).

Recently, Giampaolo and Lombardi (1994) found a difference in the dehydration behavior of a large range of samples of X-type and H-type analcimes. In this study, we have continued this approach, using several techniques on two well-characterized samples to understand better the differences found.

TABLE 1. Electron microprobe analysis of analcime in weight percent, 4-nA current, 60-s count time, 20-kV voltage

Element oxide	Ideal	H type	X type	
			Natural	Lab
SiO_2	54.5	55.35	58.52	57.76
Al_2O_3	23.2	22.52	24.16	24.38
Na_2O*	14.1	13.02	3.90	4.36
FeO	—	0.02	0.33	0.58
CaO	—	0.03	0.23	0.02
K_2O	—	0.001	0.07	1.18
Total	91.8	90.94	87.21	88.28

* The Na analyses are lower than expected because of the phenomenon of Na drift (see text).

SAMPLES

Analcime from the Dippin Sill crinanite (analcime + olivine gabbro) at Clauchlands Point, Isle of Arran, Scotland, was used as the H-type analcime. Henderson and Gibb (1977) described its occurrence. The sample consisted of single crystals with good {211} faces and therefore is assumed to have grown by dissolution and renucleation from the source rock. Since the minerals in this rock are outside the field of stability of leucite, leucite is not a possible precursor to the analcime. The crushed sample contained a small amount of tetranatrolite (3%).

The X-type analcime was from a phonolitic lava flow south of Bracciano Lake, Rome, Italy. It was deduced to be secondary after leucite from its habit as a powdery aggregate with the shape of a large leucite crystal. Leucite is abundant in these rocks, and during the process of separation a large amount of leucite was found in the aggregate. As an additional check, analcime was made in the laboratory by ion exchange from natural leucite (from Quar to Miglio, Italy) using the method of Gupta and Fyfe (1975). Although the quantity thus formed was small, it was used to confirm the results from the natural sample.

The electron microprobe analyses are shown in Table 1. One item of note is the anomalously low Na count (93% of the expected value for H-type analcime, 23% for both samples of X-type analcime). The kinetics of Na drift during analysis that caused this effect is discussed below.

In order to check for crystal strain in X-type analcime (as might be produced by the 10% expansion for solid-state ion exchange), a high-resolution X-ray diffraction experiment was carried out in which the FWHM of the strongest reflection, the {400} at 26° 2θ, was measured accurately. The instrumental resolution, as measured by the FWHM of the Si {211} peak at 28° 2θ, was 0.148° 2θ. Since the final diffraction peak is a convolution of the instrumental resolution with the sample broadening, the final width is approximately the sum of the component

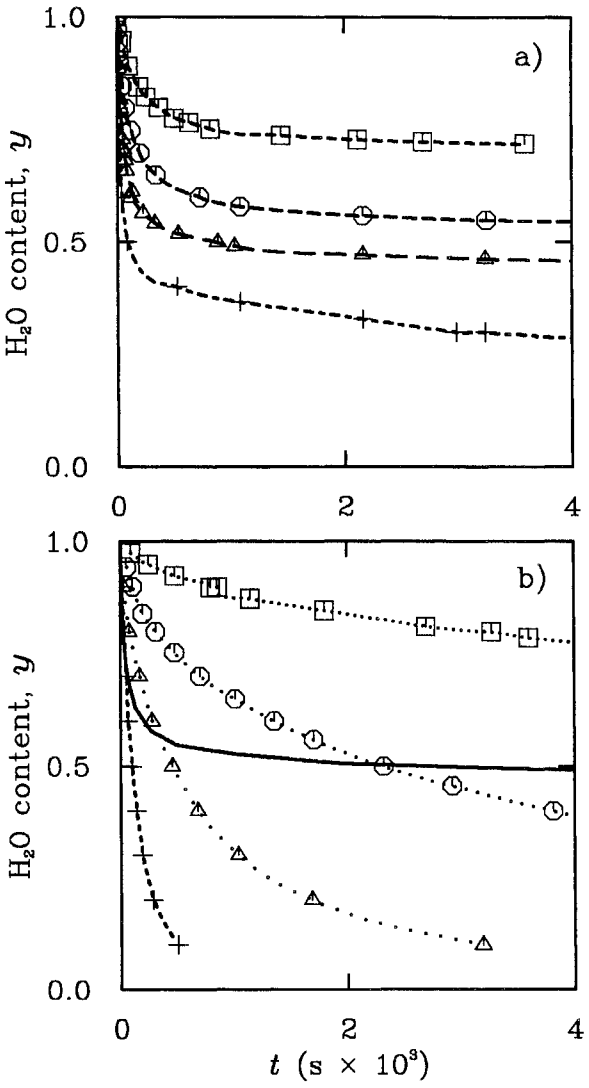

Fig. 1. H_2O content of analcime, taken relative to dry weight at 650 °C as a function of time and temperature. The dotted lines are interpolated from the data. Squares = 200 °C; circles = 250 °C; triangles = 300 °C; plus signs = 350 °C. (a) X-type analcime, (b) H-type analcime: solid line, finely pulverized H-type analcime at 250 °C.

widths. The FWHMs for H-type, natural X-type, and laboratory X-type analcime, respectively, were 0.161, 0.137, and 0.147° 2θ and hence showed no broadening. In the course of the thermogravimetry work (see below) H-type analcime was pulverized to give a large surface area. The resulting FWHM was 0.243° 2θ, which means that the width due to sample broadening was 0.082° 2θ, which could have been caused by a crystal strain of $\cot\theta\,\Delta\theta$ (in radians) = $\delta a/a$ = 0.33%. Thus the technique can detect very small crystal strains. Clearly, if any strain exists in the X-type analcime, it is much less than this value. The minimum linear strain in X-type analcime due to solid-state exchange would be 0.7% ($c_{\text{leucite}} - a_{\text{analcime}}$), and the maximum would be 5% ($a_{\text{leucite}} - a_{\text{analcime}}$). The grains of X-type analcime were also found to be optically isotropic, as expected from the cubic symmetry.

For the sample preparation, the crushed analcime grains were sieved into two size fractions, 50–75 and 75–103 μm. They were then washed in distilled water and cleaned ultrasonically to remove dust grains. They were then dried at room temperature in a desiccator using silica gel as a desiccant. For the electron microprobe analysis, samples of uniform grain size were mounted in resin, cut, polished, and coated with C. For the SEM work, both loose grains and cut and polished grains were used.

Thermogravimetry

The kinetics of dehydration was studied by isothermal weight-loss experiments in a Stanton Redcroft TG760 thermal balance. The starting sample weight (~10 mg) and the grain size (50–75 μm) were the same in each experiment, and the weight loss was recorded as a function of time at a series of temperatures, to an accuracy of 0.5%. The percentage of weight loss was determined by fully dehydrating the sample at 650 °C at the end of each isothermal experiment. Although the dehydration rate is rapid, the target temperature could be reached before appreciable H_2O loss occurred, by using a furnace in which the temperature could be increased at 1000 °C/min. A small zero-time error was incurred for the highest temperature used (350 °C), since the weight started to decrease when the temperature was at 325 °C, and the target temperature was reached 9 s later, and so for X-type analcime the first 20% of the H_2O had been lost between 325 and 350 °C. For the lower temperatures and for H-type analcime, this zero-time error can be considered to be insignificant. Sample temperature was controlled to within 1 °C. Experiments were carried out in a flowing N atmosphere, at a flow rate of ~0.3 cm^3.

X-type analcime contained H_2O in excess of the stoichiometric amount, as calculated from the dry weight at 650 °C. At room temperature the total H_2O content was 120–130% of the stoichiometric amount, and even when heated at 100 °C overnight, the H_2O content remained at 110–113% of the stoichiometric amount. By incrementally increasing the temperature, the stoichiometric amount was attained at 130 °C. H-type analcime did not have significant excess H_2O, consistent with X-type analcime having a higher surface area, even though the overall grain size is the same. In order to be able to compare the dehydration behavior of structural H_2O for the two samples, surface H_2O was eliminated by keeping both samples at 130 °C until their equilibrium weight was achieved.

The initial H_2O loss is more rapid for X-type analcime than H-type analcime. This rapid dehydration could only be reproduced in H-type analcime by using submicrometer grain sizes, attained by pulverizing H-type analcime in an agate ball mill. This is shown in Figure 1b. This observation is consistent with X-type analcime having a much higher specific surface area. The crystal strain

(0.33% $\Delta a/a$) in the pulverized H-type analcime, as deduced by the diffraction results, would seem to be too small to affect the dehydration rate, and in any case no crystal strain was detectable in the X-type analcime.

The long-term H_2O loss was also different for the two analcimes. H-type analcime, in the 50–75 μm grain fraction, lost H_2O continuously at a decreasing exponential rate, until all the H_2O was lost. This was true at all temperatures (Fig. 1b). On the other hand, dehydration in X-type analcime (Fig. 1a) did not go to completion but equilibrated at each temperature to a constant weight, even though the dehydration was under a continuous N gas flow. This behavior indicates that a local H_2O vapor pressure equilibrium is set up in the sample and that the gas flow over the sample surface was not effective at removing the H_2O vapor from the sample surface. This was true even when a faster gas flow rate was used. Since this behavior is also seen in the pulverized H-type analcime (Fig. 1b), this effect is pronounced if there is a large specific surface area, possibly because the H_2O vapor is trapped in the sample. For the purposes of the subsequent analysis, the data for X-type analcime were renormalized to each asymptotic value y_{∞}, by replacing the reaction variable y by a new variable y_{rel}, where $y_{rel} = (y - y_{\infty})/(1 - y_{\infty})$ and $y_{\infty}(T)$ is the final H_2O content.

In order both to assess the difference in activation energies and to gain some indication as to any difference in mechanism for the dehydration, attempts were made to fit the data to a series of solid-state rate equations. The data do not fit the first-order law $dy/dt = ky$, [where y is the fraction of H_2O remaining, k is the rate constant, given by $k = \tilde{k}\exp(E/RT)$, and t is time], although first-order kinetics has been observed for zeolites (Dondur and Vučelić, 1983). An equation that parameterizes many solid-state reactions is the Avrami equation:

$$\frac{dy}{dt} = yk^n t^{(n-1)} \tag{1}$$

which integrates to

$$y = \exp(-kt)^n \tag{2}$$

and is linearized by

$$\ln(-\ln y) = n \ln k + n \ln t \tag{3}$$

such that k still has, as is conventional, the dimensions of t^{-1}. Empirically, values of n can be related to the reaction mechanism for a wide range of solid-state reactions (Hancock and Sharp, 1971). Values of $n < 1$ are related to diffusion mechanisms, whereas values >1 indicate that the rate of reaction is controlled by the speed of the phase boundary.

This equation (Fig. 2a) fits the data quite well, but both plots have a negative curvature, which is more pronounced for X-type analcime. According to Burke (1965), data that give a negative curvature for the Avrami equation give an improved fit with the Austin-Rickett equation:

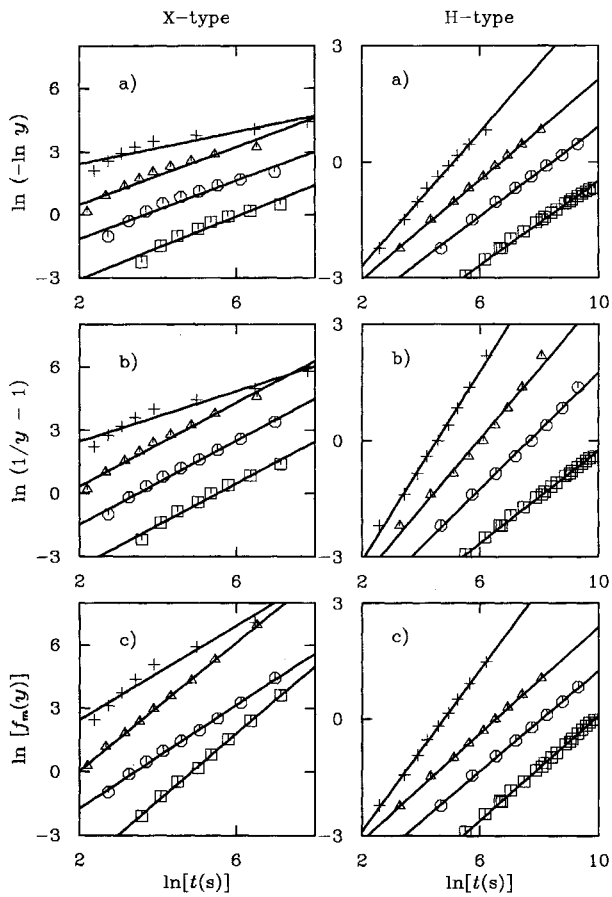

Fig. 2. Plot showing the straight-line fit of the dehydration data to three models, for all temperatures. For X-type analcime, the reaction variable is taken relative to the asymptotic value y_{∞} by replacing y by $y_{rel} = (y - y_{\infty})/(1 - y_{\infty})$. (**a**) Avrami model (Eq. 3), (**b**) Austin-Rickett model (Eq. 6), (**c**) general model (Eq. 10) such that $f_m(y) = [1/(m-1)][(1/y^{m-1}) - 1]$. Parameters n and m from Table 2. Symbols as in Fig. 1.

$$\frac{dy}{dt} = -y^2 k^n t^{(n-1)} \tag{4}$$

which integrates to

$$\left(\frac{1}{y} - 1\right) = (kt)^n \tag{5}$$

and is linearized by

$$\ln\left[-\ln\left(\frac{1}{y} - 1\right)\right] = n \ln k + n \ln t. \tag{6}$$

This equation, though giving a slightly poorer fit for the H-type analcime, gave an improved fit for the X-type analcime (Fig. 2b). This can be seen quantitatively by the differing residuals (Table 2). By plotting the extracted rate constants in an Arrhenius plot, such that $\ln k = \ln \tilde{k} - E/RT$, the activation energies can be extracted. It can also be seen that despite the differing quality of the fit, both equations give similar activation energies. Although the

TABLE 2. Parameters extracted for dehydration kinetics of H-type and X-type analcime, for general model (Eq. 10) with various values of m

	General model				Avrami model ($m = 1$)			Austin-Rickett model ($m = 2$)		
T (°C)	m	n	ln k	S	n	ln k	S	n	ln k	S
					H-type analcime					
200	2.99	0.65	−10.02	0.003	0.51	−11.1	0.03	0.58	−10.5	0.02
250	1.41	0.65	−8.06	0.03	0.58	−8.4	0.03	0.76	−7.6	0.07
300	1.18	0.69	−6.53	0.02	0.65	−6.7	0.03	0.90	−5.9	0.14
350	1.51	1.04	−4.78	0.03	0.87	−5.1	0.07	1.22	−4.5	0.09
E (kJ/mol)			81 ± 4			93 ± 2			93 ± 5	
ln [k(s^{-1})]			11 ± 1			14 ± 1			14 ± 1	
					X-type analcime					
200	3.91	1.58	−4.84	0.07	0.75	−6.1	0.20	0.99	−5.5	0.17
250	2.62	1.22	−4.39	0.08	0.69	−5.4	0.20	0.99	−4.7	0.10
300	3.36	1.52	−3.54	0.05	0.69	−4.8	0.24	0.99	−4.1	0.17
350	3.81	1.16	−3.11	0.33	0.45	−5.1	0.36	0.66	−4.1	0.35
E* (kJ/mol)			28 ± 3			29 ± 6			32 ± 8	
ln [k(s^{-1})]			2.5 ± 1			1.5 ± 0.02			2.8 ± 0.2	

Note: S = standard deviation, such that $S^2 = \frac{1}{n} \Sigma\, d_i^2$, where $d_i = Y_i - MX_i - C$, and M and C are the gradient and intercept of the straight-line fit, $Y_i = \ln(y_{i-1}^{-1} - 1)$, and $X_i = \ln t$. The errors are calculated from the fitting statistics according to Squires (1985). Unless otherwise indicated, the accuracy is to the last significant figure.

* Because of the poorness of the fit for 350 °C, the activation energy and preexponential factors for X-type analcime have been calculated for the first three temperatures only.

value of n for X-type analcime (Table 2) might indicate that a simple second-order equation (for $n = 1$) is appropriate, it is worth testing first whether the Austin-Rickett model is in fact the best solution.

The second-order nature of the reaction could be an effect of the surface desorption. Langmuir (1916) was the first to point out that the probability of m sites on the surface being occupied and adjacent to one another is θ^m, where θ is the fraction of sites occupied. If the process of desorption requires that m molecules be adjacent to one another, then the rate of desorption is given by

$$-\frac{d\theta}{dt} = k\theta^m. \tag{7}$$

Clearly for this experiment, θ is related to y, the amount of H_2O in the analcime, and if the surface has the same H_2O concentration as the bulk, θ and y are simply proportional to each other. To generalize the Austin-Rickett equation, one could envisage a general desorption-diffusion equation of the form

$$-\frac{dy}{dt} = y^m k^n t^{n-1} \tag{8}$$

where m is related to the desorption and n to the diffusion. This equation has as yet no physical basis, since it is not established that the rates for two mechanisms of desorption and diffusion would be multiplicative. Moreover, at first sight it would seem that a unique solution would be impossible to obtain, since there are two parameters in the model, as opposed to one for each of the Austin-Rickett and Langmuir equations. However, if the equation is integrated to

$$\frac{1}{m-1}\left[\frac{1}{y^{(m-1)}} - 1\right] = (kt)^n \tag{9}$$

and the logarithm of both sides is taken, as for the Austin-Rickett model, then the following is obtained:

$$\ln\left(\frac{1}{m-1}\left[\frac{1}{y^{(m-1)}} - 1\right]\right) = n \ln k + n \ln t. \tag{10}$$

The gradient of the plot, for a given value of m, gives the parameter n. Essentially, m is an independent variable, and n is the dependent variable. As can be seen from a comparison of the Austin-Rickett and Avrami plots for the data, m controls the curvature of the logarithmic plot, and n is simply the gradient of the plot. The optimal value of m is the one that gives the straightest line.

The straightness of the line was measured by the standard deviation S, calculated by $S^2 = \frac{1}{n} \Sigma_i d_i^2$, where $d_i = Y_i - mX_i - c$, and Y_i and X_i are the ordinates of the linear plot, as calculated from the model. Hence, S is model dependent, but where the ordinates X_i and Y_i are similar, the successive values of S can probably be compared. A least-squares algorithm, described by Squires (1985), gives not only the gradient and intercept of the plot but also the associated errors, since they are primarily determined by the goodness of fit. The errors associated with the individual data points are by comparison insignificant.

This refinement of m against the residual to the straight-line fit was accordingly carried out by a computer program written for the purpose, and the values of m and n for the two types of analcime are shown in Table 2, with the relevant residuals. The poor fit of the data for X-type analcime at 350 °C is probably due to the large relative significance of the experimental zero-time error. The plots are shown in Figure 2c, and the Arrhenius plots of the extracted rate constants, with the Avrami and Austin-Rickett models for reference, are shown in Figure 3. The difference between the two samples is most clearly ap-

parent in the values of the exponents. As can also be seen for the Avrami ($m = 1$) and Austin-Rickett ($m = 2$) equations, the results for which are given here, the value of n is very different for the two analcimes, indicating that the dehydration of H-type analcime is diffusion controlled, but the dehydration of X-type analcime is phase-boundary controlled. In addition, the value of m is a good indicator of the relative goodness of fit of the data to the Avrami and Austin-Rickett equations, since for H-type analcime it is closer to 1 than for X-type analcime. The parameter m could therefore be thought of as indicating the degree to which the reaction is desorption controlled and hence could be useful in model selection. It is probably unwise, however, to place much physical significance on the precise values of the exponents, since n is quite dependent on m, and the residual S is itself model dependent. As for the change of the exponents with temperature, it is irrelevant for the purposes of comparing X- and H-type analcime and more data would be required, with better controlled conditions, for any conclusions to be drawn.

The activation energies are clearly very different for the two processes. However, this does not necessarily mean that the two analcimes are energetically different (as might be expected if the X-type analcime had crystal strain due to a solid-state expansion), since if the above analysis is correct, the activation energies extracted would refer to two different processes, that of desorption and diffusion, respectively. Moreover, since for X-type analcime the reaction variable was taken relative to y_∞, the corresponding activation energy is due to a combination of the activation energies of both desorption and readsorption. Since the reaction is not first-order, deconvolution of the two processes is not possible.

In summary, the results are consistent with the dehydration of H-type analcime being primarily diffusion controlled, but the dehydration of X-type analcime being desorption controlled. This would be consistent with the X-type analcime having a higher surface area than H-type analcime.

Na DRIFT

During the course of characterizing the samples by electron microprobe (Table 1), it was noticed that the measured Na content was anomalously low for both H-type and X-type analcime, with X-type analcime having a much lower Na content than H-type analcime. Because this result must have been due to a difference in the rate of Na drift, there being no other cations observed to account for the discrepancy, an investigation was carried out to characterize the rate of drift for the two samples.

In electron microprobe analysis of alkali silica glass, ion content, especially for the alkali ions, does not in general remain constant with time. Lineweaver (1963) was the first to suggest a mechanism. According to this model, electrons come to rest in a layer several micrometers below the surface of the irradiated area. An electric field gradient is thereby established between this area and the conductive coating on the surface, by means of the Al electrode at the edge of the specimen, and as a result Na ions in the surface layer, or any other mobile cations, are drawn down toward the charge layer. At this greater depth, the incident electrons no longer have sufficient energy to excite the X-ray spectra of the Na, and so the Na count decreases. The brown color usually observed is due to the neutralized alkali atoms. Cation drift depends on the crystalline structure of the sample, with glasses having the highest rates of cation drift (Nielsen and Sigurdsson, 1981). On the other hand, minerals such as the pyroxene jadeite, which is chemically identical though structurally dissimilar to dehydrated analcime, has negligible Na drift and is therefore often used as a standard (for an example, see Nielsen and Sigurdsson, 1981).

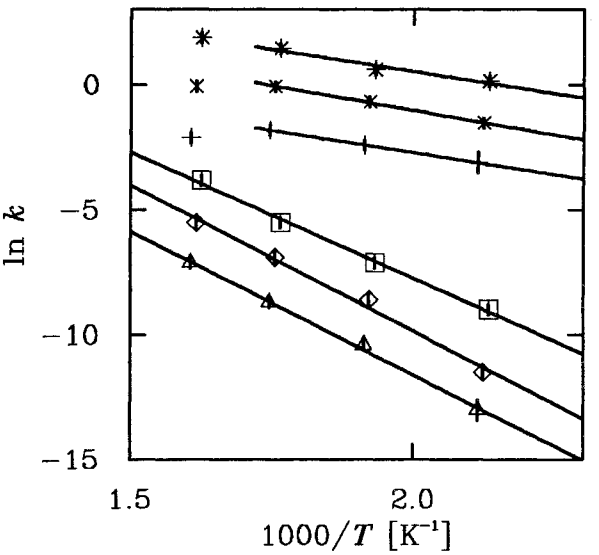

Fig. 3. Arrhenius plot of the rate constants for the dehydration curves, from Table 2. The data have been offset vertically (by 1.0) for clarity. X-type analcime: plus signs = Avrami model; Xs = Austin-Rickett model; asterisks = general model. H-type analcime: triangles = Avrami model; diamonds = Austin-Rickett model; squares = general model. The straight lines have been fitted to the data.

The electron beam has a heating effect on the specimen, which in turn increases the mobility of the ions. In a study by Vassimillet and Caldwell (1969), a temperature change of 80 °C was observed over 120 s under 50 nA and 20 kV, for a 20-μm beam diameter. In this study, a 20-kV voltage and 1-μm beam diameter were used, with currents ranging from 4 to 20 nA. It is therefore possible that dehydration occurs. This would then mean that the Na ions are more free to migrate.

With beam sizes above 10 μm, Na drift was negligible in the H-type analcime for all beam currents, though still significant in the X-type analcime. In order to compare the kinetics of drift, a small beam size (1-μm diameter) was used and the X-ray count sampled at 2-s intervals. In Figure 4a we show the raw data and the fit to the data

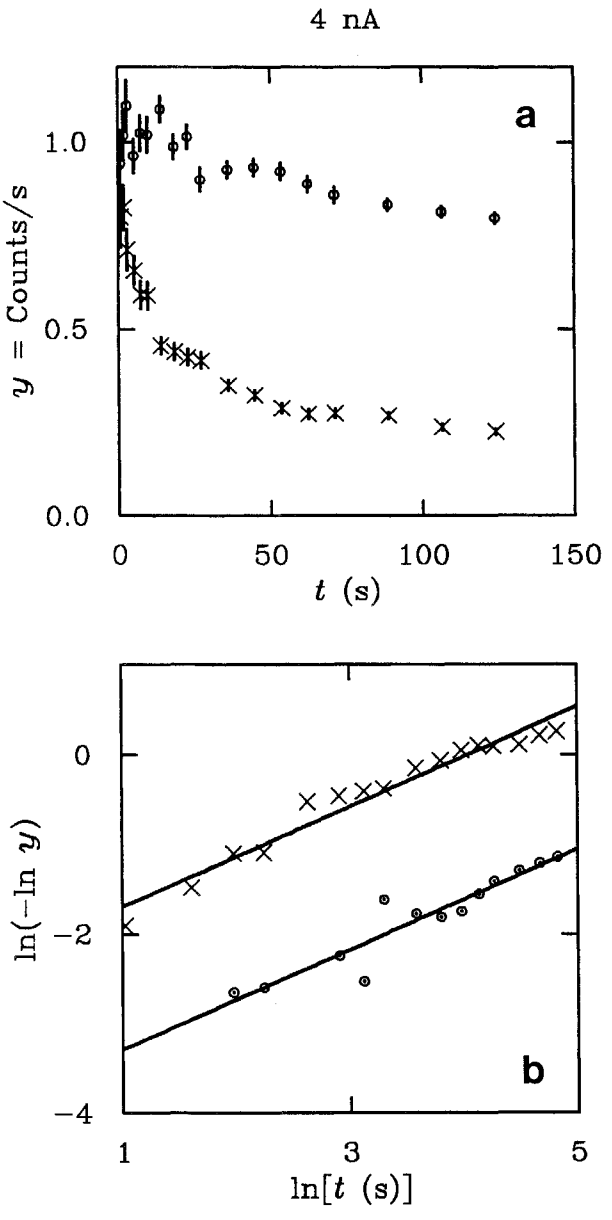

Fig. 4. Plot of the Na decay curves (**a**) and the fit to Eq. 3 (**b**), for 4-nA current and 1-μm beam size, as for Table 1. Circles = H-type analcime; Xs = X-type analcime.

for the same beam current used in the original sample characterization (Table 1). It can now be seen that the low average Na count is simply due to the high rate of Na drift in the sample and that the lower count for the X-type analcime is simply due to the higher rate of drift. Unlike the curves for Na content in glasses (Nielsen and Sigurdsson, 1981), these curves are not first-order logarithmic. However, the data do fit the Avrami equation fairly well (Fig. 4b). With the program developed for the thermogravimetry data using Equation 10, it was found that m tended to 1 (for m exactly equal to 1, the solution is of course unstable) for all the data sets, showing that the Avrami model is more appropriate than a desorption model. The extracted rate constants are shown in Table 3. The poor quality of the data, caused by the low counting statistics, means that further analysis is probably unwarranted.

Table 3. Fitted rate constants for Na drift kinetics (Eq. 3)

Beam current (nA)	H type		X type	
	ln k	n	ln k	n
4	−6.6 ± 4	0.61 ± 0.07	−4.0 ± 0.2	0.39 ± 0.02
7	−6.7 ± 0.6	0.39 ± 0.03	−4.2 ± 0.2	0.36 ± 0.01
10	−7.5 ± 1	0.23 ± 0.06	−3.4 ± 0.07	0.28 ± 0.01
20	−6.2 ± 1	0.09 ± 0.04	−2.97 ± 0.1	0.23 ± 0.01

Note: errors calculated according to Squires (1985).

As a comparative test for the two parageneses of analcime, a measurement of Na drift is useful, as it can be used on very small samples. The rate constants extracted for the two samples differ markedly. With data from the same heating current compared, it can be seen that the ratio of the rate constants, given by exp(ln k_X − ln k_H), is about 15. The change of rate constant with heating current is also far higher with X-type analcime. However, the result does not contribute to an understanding of the origin of the difference between these two parageneses of analcime, since the high Na drift in X-type analcime could be equally caused by crystal strain as by a high surface area.

Scanning electron microscopy

Scanning electron micrographs of H-type and X-type analcime, taken on a JEM 820, are shown in Figure 5. In Figure 5a and 5c, the two types are shown at similar magnifications. The H-type analcime grains are clearly single crystals, with some regular {211} faces visible in the center of the micrograph. There are some laminations that could result from different phases of crystal growth. In contrast, the X-type analcime grains do not appear to be single crystals but do appear to be polycrystalline. At higher magnification (Fig. 5d) the roughness of an apparently smooth surface of X-type analcime is shown, suggesting that the roughness is present at all scales. The roughness has become more regular, with a cauliflower appearance. This porous cauliflower texture has been observed for specimens where recrystallization has occurred. In Figure 5b, which shows an enlarged section of Figure 5a, the regular laminated texture of H-type analcime is shown, in contrast to the isotropic texture of the X-type analcime.

Finally, Figure 5e, which is a cut and polished X-type analcime grain, shows that the polycrystalline nature persists to the interior of the grain but that the texture is less visible, even when using backscattered electrons. A regular texture was only observed at magnifications of 30000, and a corresponding length scale of 1000 Å, although

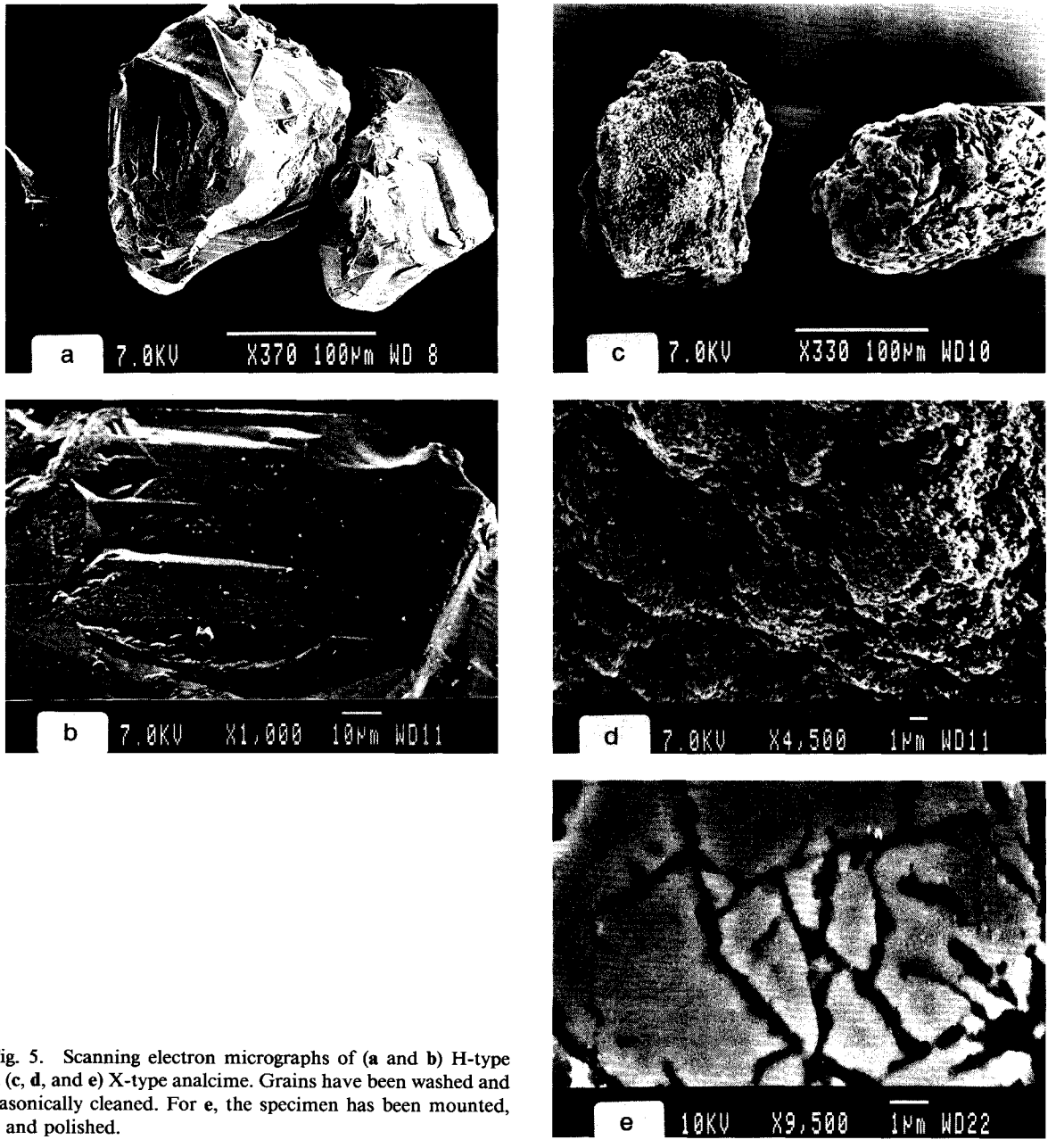

Fig. 5. Scanning electron micrographs of (**a** and **b**) H-type and (**c**, **d**, and **e**) X-type analcime. Grains have been washed and ultrasonically cleaned. For **e**, the specimen has been mounted, cut, and polished.

extensive cracks can be observed at these lower magnifications.

Electron micrographs of leucite and the X-type analcime formed in the laboratory from the same leucite sample are shown in Figure 6. The laminations in the leucite (Fig. 6a) are probably twin planes. This laboratory X-type analcime (Fig. 6b) shows a porous texture similar to that of the natural X-type analcime, consistent with formation of this porosity during the leucite-analcime reaction. Secondly, the micrographs show that the morphology of the individual grains, including the twin planes of the leucite, seems to have been preserved in the analcime formed from it. This suggests that the leucite planes may have acted as a template for the leucite-analcime reaction.

These observations show that X-type analcime does indeed have a high surface area, which is due to a porous microtexture. This would explain the anomalous dehydration properties of X-type analcime, and possibly the anomalous Na drift properties as well. Some caveats against the use of the SEM method as the sole way of distinguishing between H-type and X-type analcime stem from the observation of texture in the hydrothermal anal-

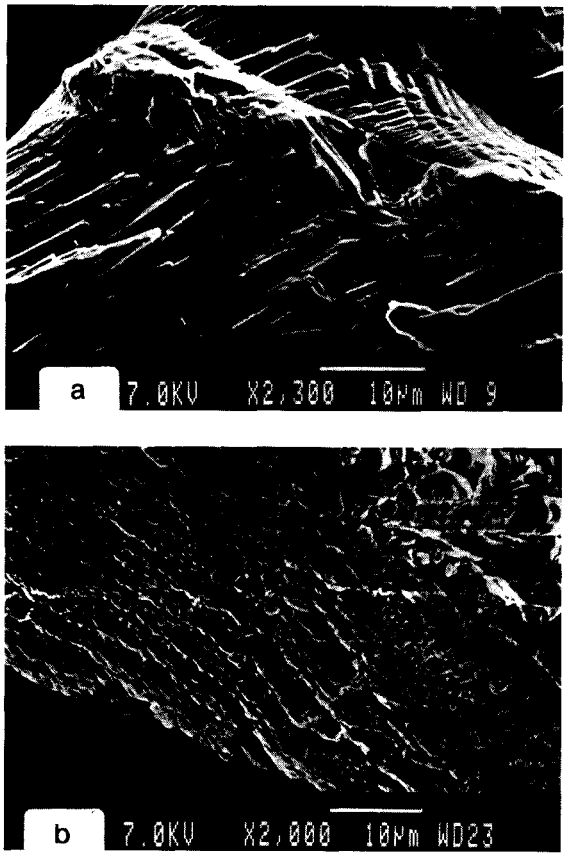

Fig. 6. Scanning electron micrographs of (a) leucite and (b) analcime formed in the laboratory by ion exchange of the same leucite sample.

cime, albeit of a much more regular and anisotropic character than in the X-type analcime.

N ADSORPTION

The N adsorption technique measures the incremental volume of N adsorbed onto the surface and absorbed into the interior of the sample, as a function of N pressure. This technique gives information on the energetics and surface area of the surface. Sing et al. (1985) summarizes the information that can be extracted, together with estimates of the associated reliability and accuracy.

The experiments were carried out on a Micromeritics Accelerated Surface Area and Porosimetry System 2000. The sample weights used were about 150 mg. For each sample, the sample chamber was first held at 100 °C (below the dehydration temperature of analcime) for 10 h before starting the N adsorption. For each data point, an incremental volume or dose of N was released into, or pumped out of, the sample chamber, and the sample equilibrated for 5 s. The resulting pressure was measured to an accuracy of 0.1% and plotted as a fraction of the measured saturation pressure, 776.346 mm Hg. The actual amount of N adsorbed was measured gravimetrically

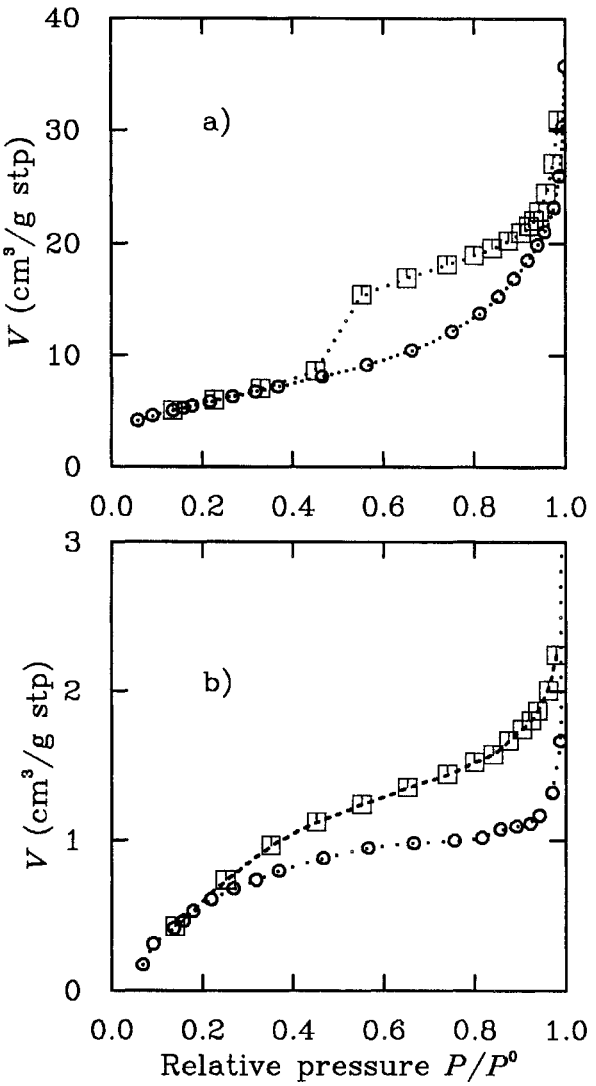

Fig. 7. N desorption curve for H-type and X-type analcime, for the small grain sizes (50–75 μm). (a) X-type analcime. (b) H-type analcime. Circles = adsorption; squares = desorption.

and converted to the equivalent volume at standard temperature and pressure, normalized to the mass of the sample.

The first feature of interest is the hysteresis in the raw data, which is present in the H-type analcime but is present to a much greater extent in the X-type analcime, shown in Figure 7. Hysteresis is observed for samples that are mesoporous, i.e., that contain pores that retain the N by capillary attraction. The curves for both X-type and H-type analcime do not exhibit any limiting adsorption at high pressures. The shape of the X-type analcime isotherm, where the adsorption branch is steep at saturation pressure and the desorption branch at intermediate pressures, is classified as Type B (de Boer, 1958; Lowell and Shields, 1984) or Type H3 (after Sing et al., 1985). It is associated with slit-like pores, or very large pores with

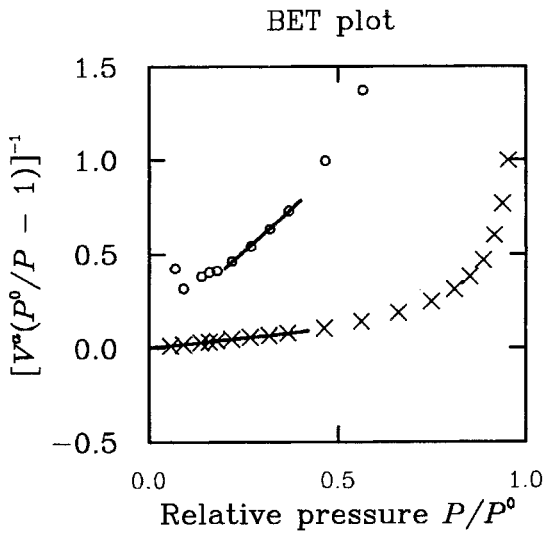

Fig. 8. BET plot of N adsoprtion data (Eq. 11) for the small grain sizes (50–75 μm). Symbols as in Fig. 4.

very small bottlenecks. The H-type analcime isotherm also has a steep adsorption branch at saturation, but the desorption branch is sloping and so is classified as Type D (de Boer, 1958; Lowell and Shields, 1984) or Type H4 (Sing et al., 1985). This type is associated with wedge-shaped capillaries. These data are consistent with the aggregate nature of the X-type analcime and the lamellar nature of the H-type analcime, as shown in the SEM micrographs (Fig. 5).

The actual amount of N adsorbed depends on the surface area of the sample. A quantitative analysis can be carried out using the BET equation. This equation, named after the originators Brunauer, Emmett, and Teller (1938) is still in use today because of its ability to predict the various adsorption curve shapes. It treats the first layer of N adsorbed as having different energetics from the subsequent layers. A simple derivation is to be found in Lowell and Shields (1984). For each pressure, the volume adsorbed is plotted as follows:

$$\frac{1}{V^a\left(\frac{P^0}{P} - 1\right)} = \frac{1}{V_m^a \cdot C} + \frac{(C-1)}{V_m^a \cdot C} \cdot \frac{P}{P^0} \qquad (11)$$

where P = pressure, P^0 = saturation pressure, V^a = amount of N adsorbed (measured here in cubic centimeters at stp). The parameter V_m^a, the volume of one single N layer, is found by fitting the equation to the data. The other parameter, C, is related to the enthalpy of adsorption by the equation $C = A_1\nu_2/(A_2\nu_1)\exp[(E_1 - L)/RT]$, where A_1 and A_2 are the probabilities of adsorption and ν_1 and ν_2 are the vibrational frequencies of the adsorbates for the first and subsequent layers respectively, E is the energy of adsorption, and L is the heat of liquefaction. From V_m^a, the monolayer volume, the surface area can be calculated by assuming that the N monolayer is close-packed.

Table 4. BET analysis results (Eqs. 11 and 12)

Grain size (μm)	BET C	BET $A_{monolayer}$ (m^2/g)	BJH A_{tot} (m^2/g)	BJH Pore V (cm^3/g)
		H-type analcime		
50–75	30	2.37	2.73	0.0038
75–100	15	2.15	2.25	0.0033
		X-type analcime		
50–75	90	20.8	21.93	0.059
75–100	50	24.4	26.89	0.045

In this study, the accepted value of 0.162 nm^2 (Sing et al., 1985) was used for the molecular cross section. According to Parks (1990), with this value for the molecular cross-section, the BET surface area closely approximates the actual surface area for most silicates.

The fit of the data to the BET equation is shown in Figure 8, and the resulting fitted values are shown in Table 4. A rough calculation shows that the surface area to volume ratio of H-type analcime, when one uses a density of 2.24 g/cm^3, is about 42 times the area calculated for 50-μm spheres. This ratio is higher than what could be accounted for by the laminations seen in Figure 5b, and so it is probably a result of the adsorption of N into the microporous zeolitic pores. The BET surface area of X-type analcime is ten times that of H-type analcime (Fig. 8, Table 4). The results from both grain sizes—the plots for the large grain sizes, being similar, were omitted earlier for brevity—can be used to estimate the error in the determination, since with such a rough surface the effect of grain size on surface area will be negligible. As can be seen from Table 4, the results give similar values for the BET surface areas for the two grain sizes but show that there are large inconsistencies in the determination of C.

Further analysis of the results yields a value for the mean pore size. This analysis uses the Kelvin equation, which models cylindrical pores:

$$\ln\frac{P}{P_0} = -\frac{2\gamma\overline{V}}{rRT} \qquad (12)$$

where P is the equilibrium vapor pressure of the liquid contained in a pore of radius r, P_0 is the equilibrium pressure of the same material at a plane surface, $\gamma = 8.85 \times 10^{-7}$ J/cm is the surface tension, and $\overline{V} = 34.6$ cm^3 is the molar volume of the liquid. This equation assumes a zero contact angle of the adsorbed liquid with the pore wall.

The equation shows that as pressure is increased, the smaller pores are filled first and then the larger pores. The observation of two branches (Fig. 7) requires that one branch corresponds to a disequilibrium situation. For this analysis, the adsorption isotherm was taken, since the very steep slope of the desorption isotherm just above the low-pressure point of closure indicates that there are some pore blocking effects, and so the desorption is not at equilibrium.

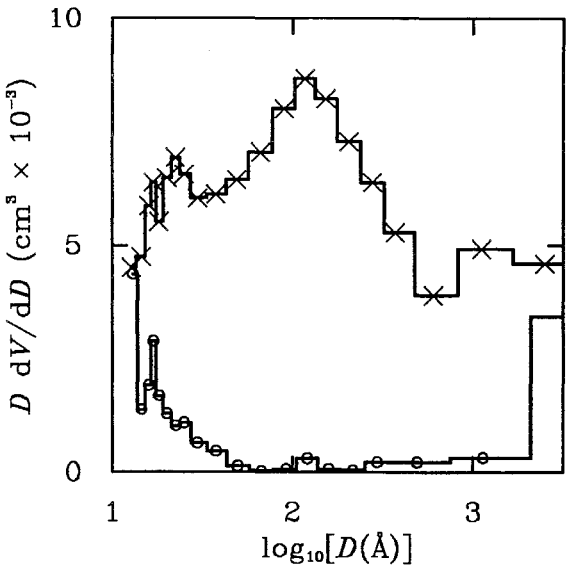

Fig. 9. Pore-size distribution from N adsorption data, for the small grain sizes (50–75 μm), using BJH method. Symbols as in Fig. 4.

Analysis of the pore size distribution was performed iteratively using the BJH method, named after Barrett, Joyner, and Halenda (1951). The final result is a plot of $D\mathrm{d}V/\mathrm{d}D$ against $\log_{10} D$, where D is the mean pore diameter, and is shown in Figure 9. It can be seen at small length scales that the zeolitic micropores are present both in H-type and X-type analcime. The difference between H-type and X-type analcime is in the presence of mesopores with a mean size of 100 Å. This pore size is below the resolution of the SEM and shows that the length scale of the microstructure is very small indeed. This pore analysis also gives values for the total pore volume and total pore surface area, calculated for pore sizes between 17 and 3000 Å in diameter. These are presented in Table 4 and provide a useful check on the BET surface areas. It can be seen in addition that X-type analcime is ten times as porous as H-type analcime.

In summary, the BET method has been shown to give a good characterization of the microtexture of analcime and provides a quantitative measure of the relative surface areas of H- and X-type analcime. The origin of the high surface area is seen to result from porosity at all scales, with a maximum in the pore-size distribution of 100 Å.

Discussion

The main thrust of this paper has been simply to demonstrate the difference in dehydration and Na drift kinetics between H-type and X-type analcime and to show that this could be simply due to the difference in microtexture and hence surface area. However, there are clues for a possible explanation for the origin of the microtexture of X-type analcime, in terms of the mechanism of the leucite-analcime reaction. The two possibilities mentioned in the introduction were solid-state ion exchange, and dissolution, renucleation, and growth from hydrothermal solution. The first, in view of the 10% volume expansion, would involve large structural strains; this is unlikely in view of our diffraction results, which show that the variation in lattice spacing must be less than $\Delta d/d = 0.3\%$ and that the grains are all optically isotropic. Moreover, X-type analcime is, due to its porosity, actually less dense than H-type analcime; one would perhaps expect that the microtexture produced by a forced expansion would show large stress cracking. The second mechanism, renucleation of analcime, would seem to be difficult in view of the kinetics, since, as explained in the introduction, grains of only a few micrometers could be grown in the small time of the reaction, and in any case the SEM results show that the laboratory X-type analcime seems to have preserved the shape of the leucite grains.

However, there is a possible third explanation, which depends on the fact that leucite, the source material for X-type analcime, has an aluminosilicate framework structure identical to analcime. This means that subunits of the leucite structure—analogous to the analcime subunits hypothesized by Ueda and Koizumi (1979)—could dissolve locally, exchange ions with the salt solution to form analcime subunits, and then nucleate straight back onto the leucite surface, rather than forming separate nuclei of analcime. Of course, the 10% change in volume would mean that there would be a structural mismatch at the leucite-analcime boundary. This would set a limit to the size of nuclei that could be formed on the leucite surface and hence would explain the extremely small scale of the microtexture. Subsequent dissolution would eventually dissolve the original leucite surface from underneath. This would explain the SEM observation that the shape of the leucite crystal has been preserved and also explain why the leucite-analcime reaction requires dilute H_2O (Gupta and Fyfe, 1975), as mentioned in the introduction. The difference between H-type and X-type analcime would lie in the structural similarity of the source material to the final material, since if the source material is structurally dissimilar (H-type analcime), then the analcime can only crystallize onto new analcime nuclei, and so this unusual microtexture would not be produced.

The level of reorganization of the aluminosilicate framework during analcimization could be checked by monitoring the change in the Al-Si order. If indeed the leucite-analcime reaction is a recrystallization reaction rather than a solid-state ion-exchange reaction, then one would expect complete Al-Si disorder in the analcime, relative to that of leucite, since the crystal growth is so fast. Thus one would expect any Al-Si order in the parent leucite to be destroyed. This prediction is yet to be checked by NMR measurements.

In any case, it can be stated fairly confidently that the X-type analcime we have observed can be characterized by this unusual microscopic texture, and thus the meth-

ods presented above could be used for determining whether other analcimes have been formed from leucite. This may be useful to the debate over the origin of igneous analcime, particularly since two of the methods employed—SEM and electron microprobe—can be used on very small samples.

Acknowledgments

C.M.B.L. would like to acknowledge a research studentship from the Institut Laue-Langevin, Grenoble, France.

References Cited

Barrer, R.M., and White, E.A.D. (1951) Hydrothermal chemistry of silicates: Synthetic lithium aluminosilicates. Journal of the Chemical Society, 1267–1278.

——— (1952) The hydrothermal chemistry of silicates: II. Synthetic crystalline sodium aluminosilicates. Journal of the Chemical Society, 1561–1571.

Barrett, E.P., Joyner, L.G., and Halenda, P.A. (1951) The determination of pore volume and area distributions in porous substances: I. Computations from nitrogen isotherms. Journal of the American Chemical Society, 73, 373–380.

Brunauer, S., Emmett, P.H., and Teller, E. (1938) Adsorption of gases in multimolecular layers. Journal of the American Chemical Society, 60, 309–319.

Burke, J. (1965) The kinetics of phase transformations in metals, 226 p. Pergamon, Oxford, U.K.

de Boer, J.H. (1958) The shapes of capillaries. In D.H. Everett and F.S. Stone, Eds., The structure and properties of porous materials, p. 68–94. Butterworths, London.

Dondur, V., and Vučelić, D. (1983) An approach to the kinetics of water desorption from A-zeolites: I. Isothermal and non-isothermal desorption. Thermochimica Acta, 68, 91–99.

Giampaolo, C., and Lombardi, G. (1994) The thermal behaviour of analcimes from two different genetic environments. European Journal of Mineralogy, 6(2), 285–289.

Gottardi, G., and Galli, E. (1985) Natural zeolites. In Minerals and Rocks, vol. 18, 409 p., Springer-Verlag, Berlin.

Gupta, A.K., and Fyfe, W.S. (1975) Leucite survival: The alteration to analcime. Canadian Mineralogist, 13, 361–363.

Hancock, J.D., and Sharp, J.H. (1971) Method of comparing solid-state kinetic data and its application to decomposition of kaolinite, brucite, and $BaCO_3$. Journal of the American Ceramic Society, 55(2), 74–77.

Henderson, C.M.B., and Gibb, F.G.F. (1977) Formation of analcime in the Dippin Sill, Isle of Arran. Mineralogical Magazine, 41, 534–537.

Karlsson, H.R., and Clayton, R.N. (1990a) Oxygen isotope fractionation between analcime and water: An experimental study. Geochimica et Cosmochimica Acta, 54, 1359–1368.

——— (1990b) Oxygen and hydrogen isotope geochemistry of zeolites. Geochimica et Cosmochimica Acta, 54, 1369–1386.

——— (1991) Analcime phenocrysts in igneous rocks: Primary or secondary? American Mineralogist, 76, 189–199.

——— (1993) Analcime phenocrysts in igneous rocks: Primary or secondary?—Reply. American Mineralogist, 78, 230–232.

Langmuir, I. (1916) The constitution and fundamental properties of solids and liquids. Journal of the American Chemical Society, 38, 2221.

Lineweaver, J.L. (1963) Oxygen outgassing caused by electron bombardment of glass. Journal of Applied Physics, 34(6), 1786–1791.

Lowell, S., and Shields, J.E. (1984) Powder surface area and porosity, 234 p. Powder Technology Series, Chapman and Hall, London.

Nielsen, C. H., and Sigurdsson, H. (1981) Quantitative methods for electron microprobe analysis of sodium in natural and synthetic glasses. American Mineralogist, 66, 547–552.

Parks, G.A. (1990) Surface energy and adsorption at mineral-water interfaces: An introduction. In Mineralogical Society of America Reviews in Mineralogy, 23, 133–175.

Pearce, T.H. (1993) Analcime phenocrysts in igneous rocks: Primary or secondary?—Discussion. American Mineralogist, 78, 225–229.

Sing, K.S.W., Everett, D.H., Haul, R.A.W., Moscou, L., Pierotti, R.A., Rouquérol, J., and Siemeniewska, T. (1985) Reporting physisorption data for gas/solid systems. Pure and Applied Chemistry, 57(4), 603–619.

Squires, G.L. (1985) Practical Physics, 215 p. Cambridge University Press, Cambridge, U.K.

Ueda, S., and Koizumi, M. (1979) Crystallization of analcime solid solutions from aqueous solutions. American Mineralogist, 64, 172–179.

Vassimillet, L.F., and Caldwell, V.E. (1969) Electron-probe microanalysis of alkali metals in glasses. Journal of Applied Physics, 40, 1637–1643.

Manuscript received April 11, 1994
Manuscript accepted November 7, 1994